Journal of Membrane Science 515 (2016) 86–97

Contents lists available at ScienceDirect

Journal of Membrane Science

journal homepage: www.elsevier.com/locate/memsci

Electrospun polystyrene nanofibrous membranes for direct contact membrane distillation

Huizhen Ke [a,b,c], Emma Feldman [a], Plinio Guzman [a], Jesse Cole [a], Qufu Wei [b], Benjamin Chu [a], Abdullah Alkhudhiri [d], Radwan Alrasheed [e], Benjamin S. Hsiao [a,*]

[a] Department of Chemistry, Stony Brook University, Stony Brook, NY 11790, United States
[b] Key Laboratory of Eco-Textiles, Ministry of Education, Jiangnan University, Wuxi, Jiangsu 214122, China
[c] Fujian Engineering Research Center for Textile and Clothing, Faculty of Clothing and Design, Minjiang University, Fuzhou, Fujian 350108, China
[d] National Center for Nanotechnology, King AbdulAziz City for Science and Technology, Riyadh, Saudi Arabia
[e] Research Institute for Water and Energy, King AbdulAziz City for Science and Technology, Riyadh, Saudi Arabia

ARTICLE INFO

Article history:
Received 26 February 2016
Received in revised form
18 May 2016
Accepted 28 May 2016
Available online 31 May 2016

Keywords:
Polystyrene
Nanofibers
Electrospinning
Membrane Distillation
Desalination

ABSTRACT

Hydrophobic electrospun polystyrene (PS) nanofibrous membranes were developed for desalination using the direct contact membrane distillation (DCMD) technique. These membranes were prepared from electrospinning of PS solutions in N,N-dimethyl formamide (DMF) with the addition of sodium dodecyl sulfate (SDS) as a processing aid. Effects of membrane thickness and fiber diameter on the average pore size and pore size distribution of nanofibrous membranes were systematically studied by capillary flow porometer (CFP), whereas the water contact angle and membrane porosity of these membranes were determined by contact angle meter (CAM) and gravimetric method, respectively. The resulting flux rate and permeate water quality (determined by conductivity) of membranes with different thicknesses and mean pore sizes from DCMD measurements were compared with those of commercially available polytetrafluoroethylene (PTFE) membranes using four different feed solutions, including distilled water, simulated brackish water, 35 g/L NaCl solution and seawater. Effects of flow rates (i.e., 0.2 GPM, 0.3 GPM and 0.4 GPM) and feed solution temperatures (i.e., 70 °C, 80 °C and 90 °C) on the flux rate and permeate conductivity of the optimized PS nanofibrous membrane (with a mean pore size about 0.19 μm) were further investigated during a continuous 10 h DCMD operation. Additionally, the mass and heat transfer coefficients of the optimized nanofibrous membranes in the DCMD operation were calculated. The results indicated that hydrophobic PS nanofibrous membranes can be produced by electrospinning for desalination by the DCMD method, leading to some unique opportunities in off the grid applications.

1. Introduction

Safe drinking water should be considered a basic human right. To ensure the continuation of humanity, robust, sustainable and cost-effective methods to remove contaminants and toxic substances in drinking water resources must be developed, where the recent advances in nanotechnology have offered many new opportunities to meet this goal [1–3]. The present study illustrates one example of using polymeric nanofibers, fabricated by the electrospinning process, for desalination application using the membrane distillation method.

Membrane distillation (MD) is a separation technique that has some unique advantages over more conventional energy-intensive membrane-enabled techniques, such as reverse osmosis (RO) or nanofiltration (NF), for water purification from desalination of seawater and brackish water to removal of heavy metals and contaminants in food processing and wastewater treatments [1–8]. Typically, the permeate flux rate of the MD operation is substantially lower than those of RO or NF. However, the MD process possesses some unique advantages: a 100% rejection capacity of non-volatile solutes (e.g., ions, macromolecules, colloids and cells), lower operating temperatures than traditional distillation methods, lower operating pressures than pressure-driven filtration techniques (e.g. RO and NF), and no concerns with the evaporator corrosion issues. [1,3,4] Typically, there are six types of MD configuration practices: direct contact membrane distillation (DCMD), air-gap membrane distillation (AGMD), sweeping gas membrane distillation (SWGMD), vacuum membrane distillation (VMD), permeate gap membrane distillation (PGMD) and vacuum multi-effect membrane distillation (V-MEMD) [2,3]. Among these, the

* Corresponding author.
E-mail address: Benjamin.Hsiao@stonybrook.edu (B.S. Hsiao).

http://dx.doi.org/10.1016/j.memsci.2016.05.052
0376-7388/

Table 1.
The total membrane thickness (δ) (i.e., the thickness of electrospun PS layer and thickness of PET non-woven substrate (~ 86 μm) together), maximum pore size, mean pore size, porosity and average flux rate of electrospun PS nanofibrous membranes and two commercial PTFE membranes (Four kinds of feed solutions: distilled water, simulated Turkana lake water, seawater and 35 g/L NaCl, testing time: 10 h; feed solution temperature: 70 °C; cold permeate solution temperature: 17 °C; flow rate: 0.2 GMP).

Sample name	δ (μm)	Maximum pore size (μm)	Mean pore size (μm)	Porosity (%)	Feed solution			
					distilled water	Simulated Turkana lake water	Seawater	35 g/L NaCl
					Average flux rate (kg/m^{2}h)			
PS-8–1	109 ± 2	0.53	0.28 ± 0.13	82	32.3 ± 0.5	29.4 ± 0.9	× [a]	×
PS-8–2	125 ± 2	0.53	0.25 ± 0.13	83	28.5 ± 0.6	26.3 ± 0.9	×	×
PS-8–3	147 ± 4	0.44	0.19 ± 0.10	84	26.9 ± 0.5	25.7 ± 0.5	24.9 ± 0.5	19.4 ± 0.9
PS-10–1	114 ± 2	0.71	0.31 ± 0.16	85	31.9 ± 0.6	30.9 ± 0.5	×	×
PS-10–2	131 ± 4	0.68	0.29 ± 0.18	85	27.3 ± 0.5	26.3 ± 0.5	×	×
PS-10–3	154 ± 5	0.60	0.25 ± 0.17	86	23.5 ± 0.4	22.2 ± 0.4	21.7 ± 0.6	×
PTFE-1	241 ± 2	0.41	0.15 ± 0.10	80	25.9 ± 0.9	24.9 ± 1.8	23.7 ± 0.5	18.2 ± 0.8
PTFE-2	84 ± 2	0.29	0.16 ± 0.05	70	23.8 ± 0.9	21.7 ± 0.9	19.9 ± 0.8	14.3 ± 0.8

[a] increased salt leakage through the membrane

DCMD configuration is the simplest one.

In the DCMD operation, hot and cold streams are in direct contact with the membrane surface. Diffusion of liquid water containing dissolved ions across the membranes surface is forbidden due to the hydrophobic nature and small pore size (usually less than 0.2 μm) of the membrane, whereas the passage of water vapor is allowed. The mass transfer of water molecules across the membrane is thus driven by the vapor pressure difference rather than the pressure difference of the flow. The vapor pressure difference can be controlled by the temperature difference between the hot feed solution and cold permeate on each side of the membrane. In other words, the vapor pressure gradient causes the movement of water vapor molecules across the membrane, where pure water is then condensed on the cold side and contaminates are trapped in the feed solution on the hot side [2,3,9]. In general, hydrophobic microfiltration membranes having an average pore size in sub-microns, where the base materials are thermally stable, chemical resistant, and with low thermal conductivity to minimize heat loss, are suitable for the MD operation [1,3]. These base materials include polytetrafluoroethylene (PTFE), polyvinylidene (PVDF) and polypropylene (PP) [4,7]. However, it is also known the superhydrophobic nature of the membranes based on these materials will induce rapid fouling or scaling problems.

Electrospinning has proven to be a technique that can produce of nanofibrous membranes, with microfiltration characteristics, from a wide range of polymers (hydrophobic and hydrophilic). Electrospun nanofibrous membranes with hydrophobic characteristics thus can be used for MD applications due to the controllable pore size in the sub-micron scale, high surface-to-volume ratio, interconnected void structure and high porosity [10–12]. In this study, we chose polystyrene (PS) as the base material for electrospinning because it is hydrophobic, abundant, inexpensive and can be easily modified to improve the fouling and scaling resistance [13]. The aims for the current work are to demonstrate the optimization of electrospinning hydrophobic PS nanofibrous membranes with high flux rate and high rejection capacity for the DCMD operation. The study of modified PS nanofibrous membranes with anti-fouling and anti-scaling properties will be presented later.

In this paper, the relationship among the average fiber diameters, mean pore size, membrane thickness and MD performance of electrospun PS nanofibrous membranes were systematically investigated. In the MD testing, four different feed solutions, including distilled water, simulated brackish water from the Turkana lake in Kenya, 35 g/L NaCl aqueous solution and seawater were used for DCMD measurement. The average flux rate and permeate conductivity were measured for each membrane. In additional, different hot feed temperatures and different flow rates were tested in order to yield the greatest maximize the volume of the pure permeate water that can be produced, respectively. Two commercially available PTFE microfiltration membranes, typically used in the MD operation, were also tested to compare with the performance of the electrospun PS nanofibrous membranes. Finally, the mass and heat transfer coefficients of the optimized PS nanofibrous membranes were also determined from the experiments using the 35 g/L NaCl salt concentration feed solution, to gain further insight into the DCMD operation in this system.

2. Experimental

2.1. Materials

The polystyrene (PS, M_w=260,000) sample, in the particle form, was purchased from Scientific Polymer Products, Inc. The chemicals, including N, N-dimethyl formamide (DMF), sodium dodecyl sulfate (SDS), isopropyl alcohol (IPA), sodium chloride (NaCl), calcium chloride ($CaCl_2$), magnesium chloride ($MgCl_2$), potassium chloride (KCl), sodium fluoride (NaF), sodium nitrate ($NaNO_3$), sodium bicarbonate ($NaHCO_3$), sodium hydroxide (NaOH) and sodium sulfate (Na_2SO_4) were supplied by Sigma Aldrich and used as received without further purification. A polyethylene terephthalate (PET) non-woven cloth (average fiber diameter around 40 μm, membrane thickness around 86 μm), obtained from Junyaku Co., Ltd., (Japan), was selected as the substrate to support electrospun PS nanofibrous scaffold. One polytetrafluoroethylene (PTFE) membrane (GORE® Fine Filtration Products, product-number: L32233) was supplied by the SolarSpring Corporation (Germany). The other PTFE-based microfiltration (MF) membranes (product-number: QL816) were obtained from Sterlitech Corporation (USA). In this study, we labeled these two commercially available PTFE membranes as PTFE-1 (Solar Spring) and PTFE-2 (Sterlitech Corporation), respectively. The characteristics of these two commercial PTFE membranes are shown in Table 1.

2.2. Preparation of PS solutions for electrospinning

The four PS solutions of varying concentrations (i.e., 8 wt%, 10 wt%, 12 wt% and 15 wt%) were prepared by dissolving PS particles into DMF solvent. Following a period of stirring, 0.5 wt% of SDS (with respect to DMF) was added into the solution to facilitate the electrospinning operation. Subsequently, magnetic stirring was applied to form homogeneous PS solutions at different concentrations.

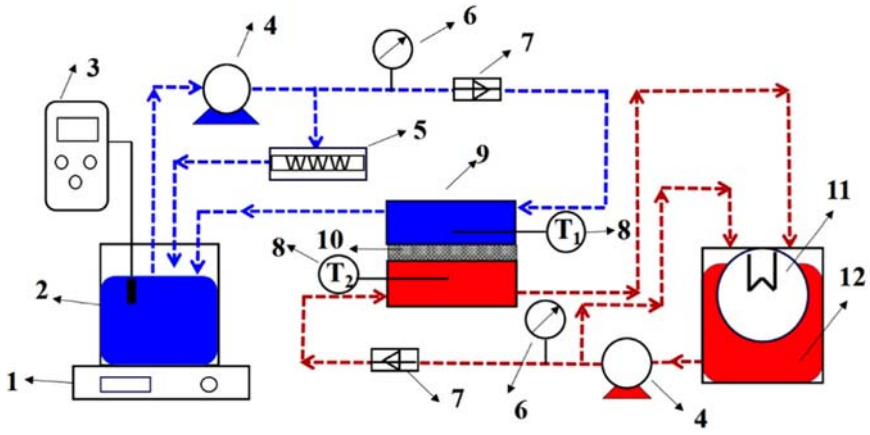

Fig. 1. Schematic diagrams of the DCMD setup: (1) digital scale, (2) hot feed solution tank, (3) conductivity meter, (4) pump, (5) chiller, (6) manometer, (7) flow meter, (8) temperature probe (T_1 and T_2), (9) DCMD cell, (10) membrane, (11) heater and (12) cold permeate solution tank.

2.3. Electrospinning to prepare nanofibrous membranes

The electrospinning setup consisted of a high voltage power supply, a syringe pump and a drum collector. Two 60 mL syringes, containing the same PS solution, were used to feed the dual electrospinning spinnerets. The inside and outside diameters of the spinneret were 0.6 mm and 0.9 mm, respectively. The collector was placed at 18 cm below the spinnerets, where the rotating speed of the collector was fixed at 100 rpm. The chosen solution delivery rate for each spinneret was 5 μL/min, modulated by the syringe pump. The applied voltage was maintained at 30 kv. Electrospun PS nanofibers were deposited onto the PET non-woven substrate (taped on the drum collector) and formed a composite nanofibrous membrane. The room temperature and relative humidity (RH) in the electrospinning chamber were kept constant at 25 °C ±2 °C and 15–18%, respectively. Several different thicknesses of the PS layer were prepared to optimize the effective pore size, porosity and filtration performance of this membrane system. The PS/PET membrane produced by using the 8 wt% PS solution was named as PS-8, where the membrane produced by the 10 wt% PS solution was named as PS-10, and so on (Table 1).

2.4. Characterization of nanofibrous membranes

2.4.1. Scanning electron microscopy (SEM)

Scanning electron microscopy (LEO 1550) with a Schottky field emission gun and Robinson backscatter detector was used to observe the surface morphology of electrospun PS nanofibrous scaffold of the membrane prepared at different PS concentration. Prior to the examination, all membranes were coated with conductive gold (Au) using a sputter coater (model SC6620) under argon atmosphere. The fiber diameter and average fiber diameter (AFD) were determined from the SEM images using the LeicaIMGRead software.

2.4.2. Capillary flow porometer (CFP)

The mean pore size and pore size distribution of electrospun PS nanofibrous membranes and commercial PTFE membranes were investigated by a capillary flow porometer (CFP-1500A, Porous Materials PMI Inc., USA), where the wetting fluid Galwick™ (Porous Materials Inc.) with a surface tension of 15.9 dynes/cm was used as the testing probe.

2.4.3. Contact angle meter (CAM)

An optical contact angle meter (CAM200, KSV instruments, LID) was used to analyze the contact angle of a water droplet on the membrane surface. In this measurement, the membrane was fixated on a glass slide, where a 5 μL water droplet was dropped on the surface of the sample. Digital images were collected using the CAM software, where the water contact angle was estimated by a curve fitting method.

2.4.4. Membrane porosity and thickness measurements

The porosity of the membrane, defined as the ratio between the volume of the pores to the total volume of the membrane, was determined by the gravimetric analysis method [14]. In this measurement, isopropyl alcohol (IPA) was used as the wetting liquid to penetrate into the pores of the membrane. Subsequently, the weight of the membrane before and after saturation with IPA was measured, and the porosity of the membrane was calculated using the following equation:

$$\varepsilon = \frac{(W_w - W_d)/\rho_i}{(W_w - W_d)/\rho_i + W_{PS}/\rho_{PS} + W_{PET}/\rho_{PET}}$$

where W_d is the weight of the dry membrane (including electrospun PS and non-woven PET layers), W_w is the weight of the wet membrane, W_{PS} is the weight of the PS layer only, W_{PET} is the weight of the non-woven PET substrate only, ρ_i is the IPA density, ρ_{PS} is the PS density and ρ_{PTE} is the PET density.

The thickness of the membranes was estimated using a micrometer. The measurements were taken from 30 different locations around the membrane and then the mean thickness was taken as the averaged value.

2.5. Direct contact membrane distillation (DCMD) testing

The electrospun PS nanofibrous membranes with different PS layer thicknesses (thus different mean pore sizes), and two commercial PTFE membranes were chosen for 10 h continuous DCMD measurement. The schematic diagram of the custom-built DCMD apparatus is shown in Fig. 1. In this study, four different feed solutions, including distilled water, simulated Lake Turkana water in northern Kenya, 35 g/L NaCl aqueous solutions and seawater (collected at the north shore of Long Island near Stony Brook) were used for the DCMD measurement. The feed solution that simulates the water from Turkana Lake (Kenya's largest lake and the world's largest desert and alkaline lake) was prepared by dissolving the following chemicals: NaCl (1070.62 mg/L), $CaCl_2$ (8.88 mg/L), $MgCl_2$ (5.73 mg/L), KCl (0.76 mg/L), NaF (32.05 mg/L), $NaNO_3$ (23.72 mg/L), Na_2SO_4 (8.43 mg/L), $NaHCO_3$ (739.2 mg/L) and NaOH (10.39 mg/L) into distilled water.

For the DCMD measurement, membranes were first cut into 10 cm × 10 cm squares with holes punched in the corners using a stamp cutter. The effective area of the membrane for DCMD testing

was 81 cm^2. The temperatures of the hot and cold streams were maintained at 70 °C ±2° and 17 °C ±2°, respectively. The flow rates of hot and cold streams were regulated at a constant rate of 0.2 GPM, which were monitored by a flow meter. The permeate conductivity and the volume of permeate water were recorded every half hour over a period of 10 h by using a conductivity meter (Oakland) and a digital balance (Pennsylvania Model 7500). The average permeation flux rate (kg/m^2h) was calculated according to the recorded weight gain of the permeate water. The pH value of the permeate water condensed during the measurement was compared to that of distilled water. In additional, the fluoride concentrations of the permeate water from the experiments using simulated Turkana lake water were specifically tested by a Extech fluoride reader to ensure that it was successfully removed by the DCMD operation (this is because Lake Turkana's water with a high level of fluoride (> 10 ppm) is unsuitable for agriculture, livestock, and domestic use). In order to compare the efficiency of electrospun PS nanofibrous membranes, two commercial PTFE membranes were also tested in DCMD under exactly the same experimental conditions. Finally, the effect of the temperature difference between the feed solution and the permeate on the flux rate and permeate conductivity using electrospun PS nanofibrous membranes were investigated (three feed solution temperatures were chosen: 70 °C ±2°, 80 °C ±2° and 90 °C ±2°, for 10 h of DCMD measurement with 35 g/L NaCl solution). In additional, salt rejection (SR) of the membranes was calculated using the following equation:

$$SR=\frac{C_f - C_p}{C_f}\times 100\%$$

where C_f and C_p are the conductivity of the feed solution and the permeate solution, respectively.

3. Results and discussion

3.1. Morphology of electrospun PS nanofibrous layer

It is well known that the surface morphology and average fiber diameter of electrospun nanofibers are functions of some important material variables, including polymer properties (e.g., type of polymer, architecture, molecular weight and distribution, and solubility), solvent properties (e.g., polarity, volatility and vapor pressure), polymer solution properties (e.g., solution concentration, viscosity, elasticity, surface tension and conductivity), electrospinning parameters (e.g., applied voltage, feed rate, collection method, and distance between the spinneret and collector), and environmental conditions (e.g., temperature, humidity and air velocity) [10–12].

The resulting morphology and average fiber diameter (AFD) of electrospun PS nanofibers have very profound effects on the membrane properties such as mean pore size and pore size distribution [15]. Based on the published membrane results for successful MD operation [3], we set a target of fabricating electrospun PS nanofibrous membranes having about 0.2 μm mean pore size and bead-free nanofiber structure. To achieve this goal, SDS, an anionic surfactant, was used to facilitate the electrospinning processing of PS solution, where the effects of polymer concentration and the addition of 0.5 wt% SDS were first investigated. The changes of viscosity, conductivity and surface tension of PS solutions as a function of polymer concentration (8 wt%, 10 wt%, 12 wt% and 15 wt%) and with/without the addition of SDS are shown in Fig. 2. It was seen that the most notable effect of SDS was the increase in solution conductivity, whereas the conductivity decreased with the increase in polymer concentration. In specific,

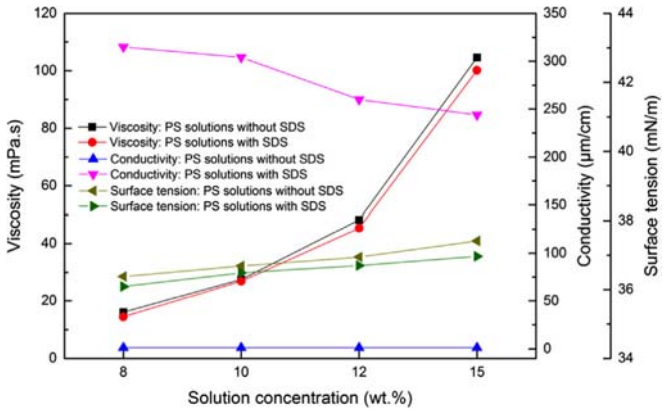

Fig. 2. Viscosity, conductivity and surface tension of PS solutions as a function of polymer concentration (8 wt%, 10 wt%, 12 wt% and 15 wt%) and with/without the addition of SDS.

the conductivities of the PS solutions without SDS were 1.08 μS/cm, 1.11 μS/cm, 1.13 μS/cm and 1.16 μS/cm for polymer solutions with concentrations of 8 wt%, 10 wt%, 12 wt% and 15 wt%, respectively. The corresponding conductivities of the PS solutions with 0.5 wt% SDS sharply increased to 315 μS/cm, 304 μS/cm, 260 μS/cm and 244 μS/cm, respectively. In additional, the SDS addition slightly decreased the surface tension and the viscosity of the polymer solution. The viscosity of the polymer solution increased sharply with the PS concentration, which was widely expected. Fig. 2 clearly illustrates the benefits of using SDS to facilitate the electrospinning of PS solutions due to the increase in conductivity (thus higher elongation during electrospinning) and decreases in viscosity and surface tension.

Fig. 3 illustrates the typical SEM images (A: without SDS, B: with SDS), AFD, fiber diameter distribution, and water contact angle (C: with SDS) of a series of PS nanofibrous membranes electrospun from solutions of different concentration (8 wt%, 10 wt% and 12 wt%). In Fig. 3(A), it was seen that a large number of beaded nanofibers were generated when the PS solutions was electrospun in this concentration range without the addition of SDS. Interestingly, the lower PS solution concentration led to more beaded structure, but finer fiber diameter. In fact, we have tested additional processing parameters (e.g. voltage, spinneret to collector distance), but we found that it was generally difficult to fabricate continuous bead-free and uniform PS nanofibers at solution concentrations below 15 wt%. This phenomenon may be explained by the fact that, at lower concentrations, the molecular entanglements are insufficient to stabilize the electrospun jet. Consequently, the contraction of the diameter of the jet driven by the surface tension caused the solution to form beads and produced beaded fibers. When the PS concentration increased from 8 wt% to 12 wt%, the diameter of the bead became larger while the distance between the beads also increased. In addition, the beads changed from a spherical shape to a spindle-like shape as a result of the increase in solution viscosity (Fig. 2). The stability of polymer jets could be improved with the increase in molecular entanglements, brought about by the increase in solution viscosity, leading to the reduction of beads and the change of the bead structure (spherical beads to spindle-like beads). But this condition also greatly increased the average fiber diameter [16–19].

In order to fabricate bead-free and uniform PS nanofibers, 0.5 wt% SDS was added in PS solutions to facilitate this aims (although we did not systematically investigate the effect of SDS concentration, a few screening studies of using SDS with different concentrations did not show drastic differences in resulting membranes). The typical SEM images of nanofibers electrospun from PS solutions at different concentrations in the presence of

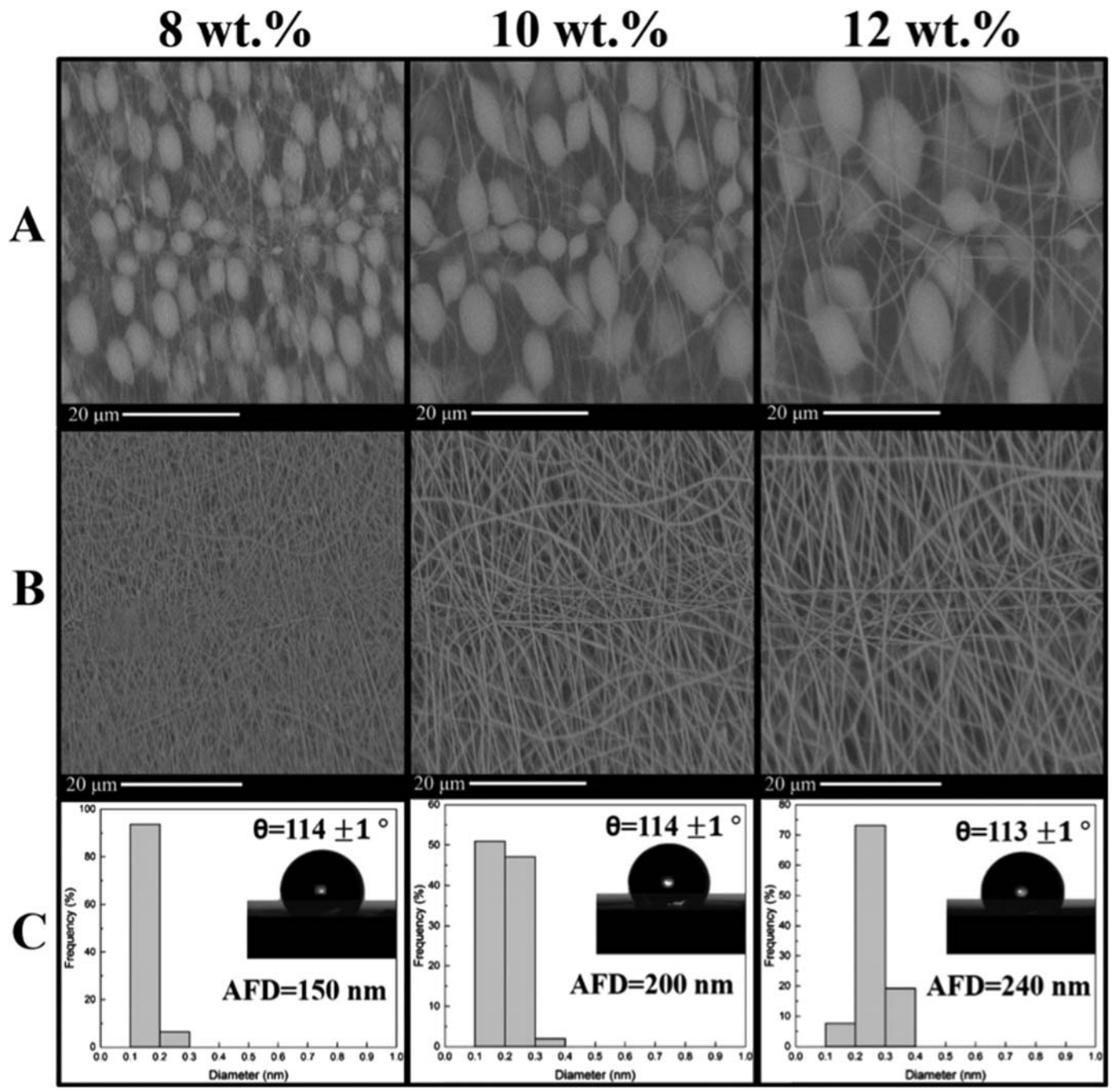

Fig. 3. Representative SEM images (A: without SDS, B: with SDS), average fiber diameter (AFD), fiber diameter distribution, and water contact angle (C: with SDS) of electrospun PS nanofibrous membranes prepared from polymer solutions at different concentrations (8 wt%, 10 wt% and 12 wt%);

SDS are shown in Fig. 3(B). These images clearly showed that the beaded structure was completely eliminated with the addition of 0.5 wt% SDS in PS solution. This behavior can be explained by the drastic increase of the conductivity in PS solutions (i.e., increase by 210–280 times with 0.5 wt% SDS) at the chosen concentration range. In specific, the increase in solution conductivity led to a larger net charge density on the electrospun jet, resulting in greater elongation forces (i.e., electrostatic or Columbic repulsion forces) on PS solution during solvent evaporation and under the electrical field. In addition, as revealed in Fig. 2, the addition of 0.5 wt% SDS also led to a slight reduction in viscosity and surface tension of PS solution, which could reduce the tendency of strong polymer aggregation that would be inductive to form bead like structure. In Fig. 3(C), it was seen that AFD of the resulting PS nanofibers decreased from 240 ± 11 nm to 150 ± 8 nm when solution concentration dropped. This behavior could be explained by the viscosity effect in electrospinning, as lower viscosity allows the Columbic forces to increase the stretching of the polymer jet. In addition, the reduced content of PS molecules in the jets at lower polymer concentration significantly reduced the average fiber diameter [17–19]. Interestingly, the water contact angles of the electrospun PS membranes prepared from different concentrations were found to be very close to each other (Fig. 3(C)). This indicates that all three membranes produced by the PS solution with SDS may be suitable for the MD operation. However, as the mean pore size is proportional to AFD, the membrane having the lower AFD value (e.g. AFD $=150$ nm) is a better candidate, which will be discussed further later. It is important to note that the

membranes with the beaded fiber structure often possessed large maximum pore size, which lacked the required quality consistency for MD operations.

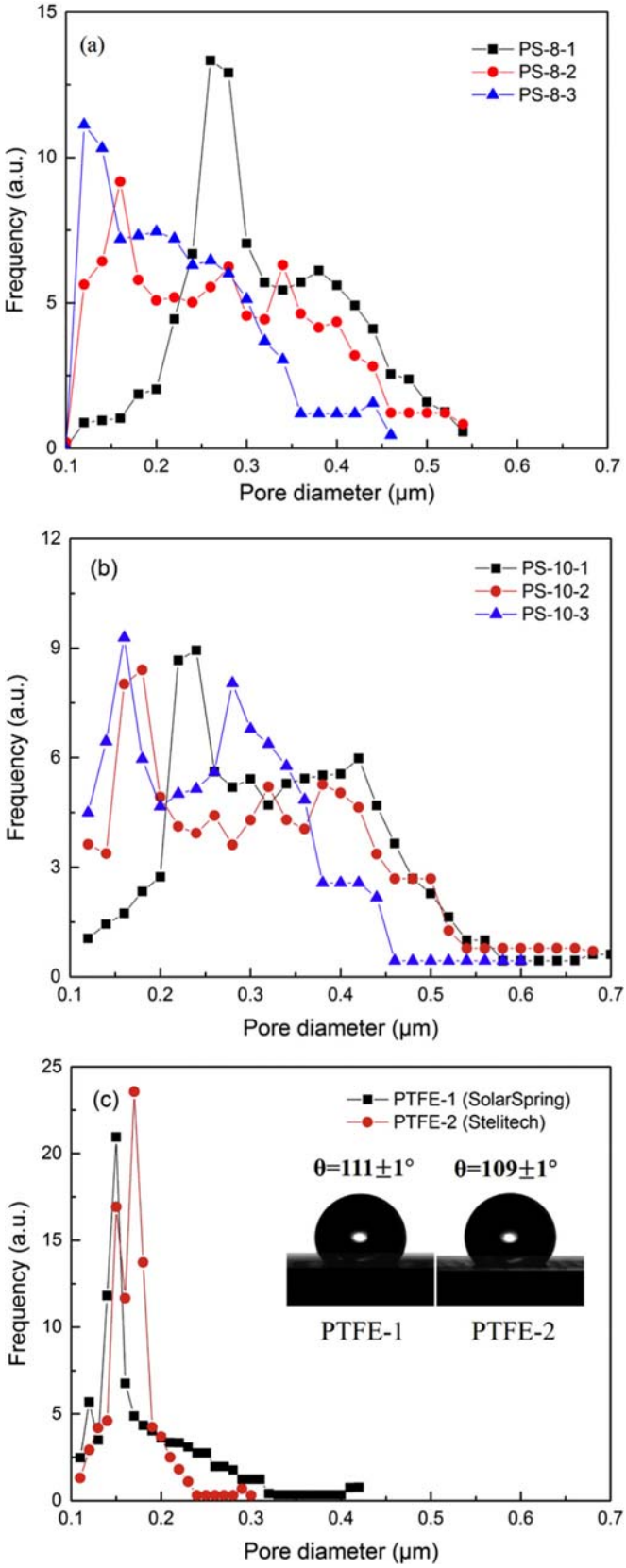

Fig. 4. The pore size distribution of electrospun PS nanofibrous membranes with different thickness and two commercial PTFE membranes. The inset in Fig. 4 (c) displays the water contact angles of two PTFE membranes.

3.2. Characteristics of electrospun PS nanofibrous membranes

The preferred pore size of hydrophobic MD membranes should be between 0.2 and 0.5 μm, based on the consideration of Knudsen and viscous diffusion for MD operation [3], and the membranes should have a uniform pore structure and high porosity. The membrane characteristics affecting the MD performance, including membrane thickness, maximum pore size, mean pore size, pore size distribution and hydrophobicity, were carefully investigated for several selected PS nanofibrous membranes produced by two lower PS concentrations (i.e., 8 wt% and 10 wt%) containing SDS in this study. The membrane thickness was obtained by three different collection times: 10 h, 17 h and 24 h during electrospinning. Figs. 4(a) and (b) show the pore size distribution obtained from nanofibrous membranes with different electrospun PS layer thicknesses prepared from 8 wt% and 10 wt% PS solutions, respectively. For comparison, the corresponding pore size distribution and water contact angle of two commercial PTFE membranes were also measured, as shown in Fig. 4(c). The relevant membrane properties such as total membrane thickness (i.e., electrospun PS layer and PET non-woven substrate layer together), mean pore size, maximum pore size and porosity for the tested samples are summarized in Table 1. It was seen that for membranes with the same ADF, the mean pore size of the electrospun PS nanofibrous membranes decreased as a result of the increase of PS layer thickness (Table 1). The pore sizes distribution curves in Figs. 4(a) and (b) were also shifted to lower and narrower value ranges with the increase in membranes thickness. As the increase in AFD, both maximum pore size and mean pore size of the nanofibrous membranes increased significantly, when the electrospinning collection time was held constant. It was interesting to note that the mean pore sizes of the nanofibrous membranes having ADF of 150 nm and 200 nm and fabricated by 24 h of electrospinning were about 0.19 μm and 0.25 μm, respectively. In was interesting to see that the pore size distributions of the electrospun PS nanofibrous membranes containing nanofibers with AFD =150 nm exhibited notably narrower pore size distribution (in the range of 0.09 μm to 0.54 μm, Fig. 4(a)) than those of the membranes containing nanofibers with AFD =200 nm (the corresponding pore size distribution in the range of 0.10 μm to 0.72 μm, Fig. 4(b)).

The porosity of electrospun PS nanofibrous membranes was found to be high (in the range of 82–86%), indicating that the optimized electrospun PS nanofibrous membranes could result in high permeation flux rate for MD operation. This was confirmed in this study and will be discussed in the next section. In Table 1, it was seen that the mean pore size and maximum pore size of the two PTFE membranes were slightly smaller than those of the electrospun PS nanofibrous membranes, but the porosities of electrospun PS nanofibrous membranes were higher than those of PTFE membranes. In addition, the water contact angles of all studied electrospun PS nanofibrous membranes were slightly higher than those of the PTFE membranes. Based on these results, the electrospun PS nanofibrous membranes with 0.19 μm mean pore size, high porosity and high hydrophobicity was chosen as a good membrane candidate for DCMD operation. The estimated liquid entry pressure (LEP) for this PS nanofibrous membrane (mean pore size about 0.19 μm and maximum pore size about 0.44 μm) was around 1.5 bar based on the method outlined earlier [3].

3.3. DCMD performance of electrospun PS nanofibrous membranes

In the present study, DCMD measurements of electrospun PS nanofibrous membranes with different pore sizes and different membranes thicknesses were carried out to determine the filtration performance (i.e., flux rate and permeate conductivity) using

four kinds of feed solutions: distilled water, simulated Turkana Lake water, 35 g/L NaCl solution and seawater for a 10 h operation. The operating temperatures for the hot feed solution and the cool permeate water were set at 70 °C and 17 °C, respectively. The flow rates at both sides were kept at a constant rate of 0.2 GPM. The results were summarized in Table 1. In this table, it was seen that the permeate flux rates decreased with the increase in membrane thickness, decrease in the maximum pore size and mean pore size under the chosen DCMD conditions for all feed solutions. In other words, the permeate flux rate of the membrane was inversely related to the membrane thinckness, but proportionally related to the maximum pore size and mean pore size of the membrane. The DCMD results using four feed solutions showed a notable effect of salt concentration on the permeate flux rate. It was seen that the permeate flux rate significantly decreased with the increase in salt concentration in the hot feed solution. This can be explained by the concentration polarization effect and the decrease of the water vapor pressure at the interface between the hot feed solution and the membrane. In Table 1, when the seawater and 35 g/L NaCl solutions were employed as the feed solutions for the 10 h DCMD testing, the permeate conductivity of electrospun PS-8–1, PS-8–2, PS-10–1 and PS-10–2 nanofibrous membranes could not be maintained below 5 μs/cm for the duration of the operation. This further confirmed the concentration polarization effect leading to the increased salt leakage through the membrane.

The data in Table 1 indicates that the electrospun PS-8–3 nanofibrous membranes, which resembled the characteristics of two commercial PTFE membranes, exhibited a higher permeate flux rate than its counterparts using all feed solutions tested. The effects of the nanofiber structure on the permeate flux rate and permeate conductivity were further investigated as follows. Fig. 5 shows the changes of the permeate conductivity for six kinds of electrospun PS nanofibrous membranes and two commercial PTFE membranes generated from the DCMD experiment using the 35 g/L NaCl feed solution. In Fig. 5, the permeate conductivity of the PS-8–3 nanofibrous membranes and two commercial PTFE membranes were completely overlapped on top of each other, which was lower than 5 μs/cm after a testing period of 10 h. The calculated SR percentage of the electrospun PS-8–3 nanofibrous membrane and two commercial PTFE membranes were $>99.99\%$. However, the permeate conductivity of other PS nanofibrous membranes was found to significantly increase with the testing

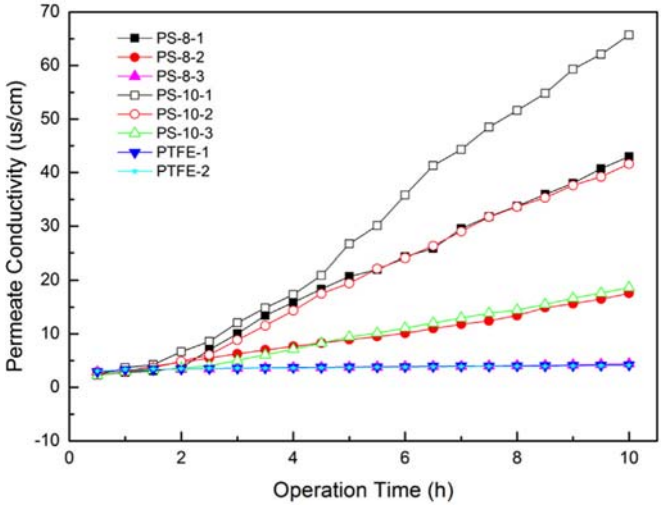

Fig. 5. The permeate conductivity of different kinds of electrospun PS nanofibrous membranes and two commercial PTFE membranes during the testing period of 10 h (the feed solution was 35 g/L NaCl, flow rate was 0.2 GPM, feed solution temperature was 70 °C, cold permeate stream temperature was 17 °C).

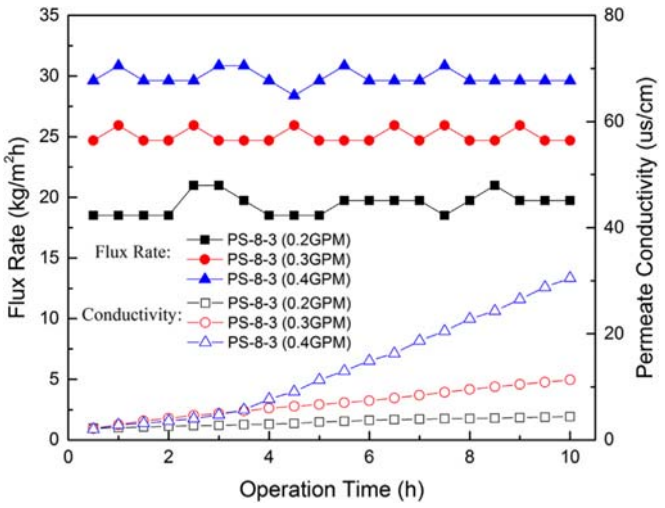

Fig. 6. The permeate flux rate and conductivity of electrospun PS-8–3 nanofibrous membranes during the testing period of 10 h with different hot feed solution temperature: 70 °C, 80 °C and 90 °C (feed solution was 35 g/L NaCl, flow rate was 0.2 GPM, cold permeate stream temperature was 17 °C).

time as a result of the concentration polarization effect leading to increased salt leakage. This occurrence was most prevalent in thinner membranes with larger pore sizes.

Fig. 6 illustrates the changes of permeate flux rate and conductivity for the PS-8-3 membrane during the DCMD operation using 35 g/L NaCl feed solution under different flow rates: 0.2 GPM, 0.3 GPM and 0.4 GPM. It was seen that although the permeate water flux rate gradually increased from 19.4 ± 0.9 kg/m^{2}h to 29.9 ± 0.7 kg/m^{2}h with the increasing flow rates of both hot and cold feed streams, the permeate conductivity also increased during the operation. This could be explained by the possibility of pore wetting on the surface of electrospun PS-8–3 membrane with the increase in flow rate.

Fig. 7 shows the changes of permeate flux rate and conductivity for the PS-8–3 membranes over the testing period of 10 h using the 35 g/L NaCl feed solution at varying temperatures: 70 °C, 80 °C and 90 °C. It was seen that the permeate flux rate increased notably from 19.4 ± 0.9 kg/m^{2}h to 31.1 ± 0.6 kg/m^{2}h with the increase in hot feed solution temperature (from 70 °C to 80 °C), which could be attributed to the increase in water vapor pressure

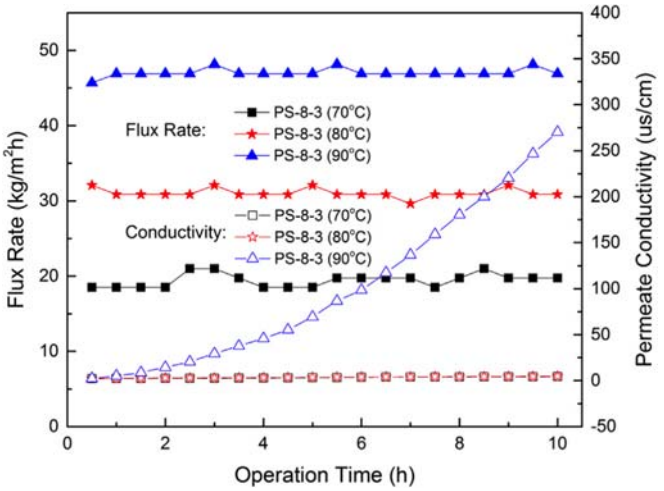

Fig. 7. The permeate flux rate and conductivity of electrospun PS-8-3 nanofibrous membrane during the testing period of 10 h at different flow rate: 0.2 GPM, 0.3 GPM and 0.4 GPM. (feed solution was 35 g/L NaCl, flow rate was 0.2 GPM, cold permeate stream temperature was 17 °C).

difference across the membrane interface. However, the pore structure of the PS-8–3 membranes might become less stable when the hot feed solution temperature reached 90 °C (it was near the glass transition temperature of PS). Based on the above results, we conclude that the suitable flow rate and the feed temperature for the DCMD operation to purify 35 g/L NaCl solution using the PS-8–3 nanofibrous membrane should be 0.2 GPM and 80 °C, respectively. The DCMD performance of PS-8–3 membrane (with 0.19 μm average pore size) seemed to be better than those of two chosen commercial PTFE membranes. Furthermore, Table 2 compares the MD performances (i.e., the flux rate (J_w) and salt rejection (SR)) of the electrospun PS-8–3 nanofibrous membrane and those of other electrospun nanofibrous membranes (ENMs) reported in the literature [14]. The results suggested that electrospun PS-8–3 nanofibrous membrane reported in this paper is consistent with the published PS data and is very suitable for MD applications.

3.4. Mass and heat transfer analysis

In this section, theoretical mass and heat transfer analyses were carried out for the PS-8-3 nanofibrous membrane for MD operation. Comparisons between the theoretical values and the experimental results may allow us to better understand the DCMD operation using these nanofibrous membranes.

3.4.1. Theoretical mass transfer analyses

During MD operation, the mass transfer across the membrane can be related to several membrane characteristics: average pore size, pore size distribution, porosity, membrane thickness and tortuosity. This process can be related to three mechanisms: Knudsen diffusion (i.e., resistance imposed by the membrane structure), Poiseuille flow (i.e., viscous flow or the momentum transfer in the membrane) and molecular diffusion (i.e., collision of molecules becomes dominant). In fact, the mass transport across the membrane (with sub-micron pore size) in DCMD has been described by all three models: Knudsen model [33], Poiseuille flow model [34] and molecular diffusion model [35]. In this study, our adaptation of using the suitable model to describe the mass transfer coefficient (and heat transfer coefficient later) of the optimized nanofibrous PS membranes in the DCMD operation is as follows.

In general, the mass transfer boundary layer resistance can be neglected, and the surface resistance is also insignificant because the surface area of the membrane is small when compared to the pore area. Often, MD membrane is fouled after a long period of operation that would greatly affect the flux rate and rejection capability. However, in this study, as the membranes were only tested for 10 h, the membrane fouling resistance could also be ignored. As both hot and cold feed streams are in direct contact with the membrane surfaces under the atmospheric pressure in the DCMD configuration, the total pressure (P) inside the membrane pore, which is equal to the sum of the partial pressures of air (P_a) and water vapor (P_v) in the membrane pore, can be assumed constant at about 1 atm. This also results in a negligible viscous flow [3,9,33,36,37].

The Knudsen number (k_n, defined as the ratio between the mean free path (λ) of the transported molecules and the membrane pore size) can provide a guideline in determining which mechanics (statistical or continuum mechanics) is relevant to describe the fluid dynamics in the membrane system. If $k_n>1$ (Knudsen region), the mean free path of the vapor molecule is larger than the membrane pore size, the continuum assumption of fluid mechanics is not suitable, while the statistical methods must be used. If $k_n<0.01$, the molecular diffusion model should be used to describe the mass transport process in the continuum region. In the transition region, i.e., $0.01 < k_n < 1$, the resistance imposed by the membrane structure is described by both Knudsen diffusion and molecule diffusion mechanisms. The mean free path (λ) of water vapor can be calculated using the following equation [3,36]:

$$\lambda=\frac{k_B T_m}{\sqrt{2}\,\pi P_{ave} d_e^2} \quad (1)$$

where k_B is the Boltzmann constant (1.38065×10^{-23} $m^2\cdot kg\cdot s^{-2}\cdot K^{-1}$), d_e is the collision diameter of the water vapor molecule (about 2.64×10^{-10} m), T_m is the average temperature (in K) in the membrane (i.e., the average between the membrane surface temperatures, $T_m=(T_{fm}+T_{pm})/2$), P_{ave} (in Pa) is the average pressure within the membrane pores (the total pressure is 1 atm for DCMD) [36]. As the surface temperatures on both sides of the membrane (i.e., T_{fm} and T_{pm}) could not be measured directly, we assumed T_{fm} and T_{pm} equal to the feed and permeate temperatures, T_f and T_p [3,4,33,37]. In addition, if we used distilled water as the feed solution, no effects of concentration and temperature polarization needed be considered. In this case, when the operating temperature of hot feed solution (T_f) was 70 °C and that of the cool

Table 2.
Comparison between the flux rate (J_w) and salt rejection (SR) of electrospun PS-8–3 nanofibrous membrane and those of other ENMs reported in the literature through DCMD measurement.

ENMs	J_w (kg/m$^2\cdot$h)	SR (%)	Q_f[a] (L/min)	Q_p[b] (L/min)	ΔT[c] (°C)	Feed solution (NaCl)	Ref.
PVDF-HFP/PAN	30	> 98.5	0.4	0.2	40	35 g/L	[20]
PVDF-HFP/CNTs	29.5	> 99.99	~0.007	~0.007	40	35 g/L	[21]
PVDF-clay NNMs	5–6	99.97	1.8	1.8	63	3.5 wt%	[22]
PVDF-HFP	13.28	99.99	0.21	0.21	55	3 wt%	[23]
PVDF-HFP	22	99.98	0.4	0.4	40	3.5 wt%	[24]
PVDF-HFP	20–21	98	15	15	41	1 wt%	[25]
SiO_2-PVDF	25	> 99.99	0.6	0.6	40	3.5 wt%	[26]
SiO_2-PVDF	41.1	> 99.99[d]	0.6	0.6	40	3.5 wt%	[27]
SiO_2-PVDF	18.9	> 99.99[d]	0.8	0.8	40	3.5 wt%	[28]
I-PVDF	31.6	–	0.4	0.6	40	3.5 wt%	[29]
PVDF	21	> 99.99	2	0.5	40	3.5 wt%	[30]
PVDF	7–28	99.9	500 rpm	500 rpm	40	3 wt%	[31]
PVDF	39	> 99.99	500 rpm	500 rpm	60	30 g/L	[32]
PS	51	> 99.99[d]	0.6	0.6	50	35 g/L	[14]
PS	31.05	> 99.99	0.2 GPM (~0.75 L/min)	0.2 GPM (~0.75 L/min)	63	35 g/L	This study

[a] The flow rate of feed solution.
[b] The flow rate of permeate solution.
[c] The temperature difference between the feed solution and permeate solution.
[d] The SR was calculated according to the data reported in the literature.

permeate (T_p) was 17 °C, the estimated mean free path (λ) of water vapor would be around 0.14 μm for the PS-8–3 membrane, which is less than the mean pore size of 0.19 μm.

If we assumed non-interconnected cylindrical pores and uniform pore radius, the mass flux rate (J_w) can be calculated as follows [36]. The value of J_w across the membrane is proportional to the mass transfer coefficient and the water vapor pressure difference across the membrane [3,36,37]:

$$J_w = C_m(P_f - P_p) \tag{2}$$

The mass transfer coefficient of the membrane C_m (kg/$m^2 \cdot s \cdot Pa$) can be determined experimentally or theoretically based on the three mass transfer mechanisms. P_f and P_p are the feed and permeate water vapor pressures of the membrane. In this study, the calculated Knudsen number was ranged between 0.01 and 1, which means that the mass transfer across the membrane takes place by both Knudsen and molecular diffusion mechanisms [33,36,37], i.e.,

$$C_m = \frac{1}{RT_m\delta}\left[\frac{3\tau}{2\varepsilon r}\left(\frac{\pi M_w}{8RT_m}\right)^{\frac{1}{2}} + \frac{P_a\tau}{\varepsilon PD}\right]^{-1} \tag{3}$$

where R is the gas constant (8.314 $J \cdot K^{-1} \cdot mol^{-1}$), δ is the membrane thickness (m),τ is the pore tortuosity (%), ε is the porosity (%),r is the pore radius (m), M_w is the molecular weight of water (1.802×10^{-2} kg/mol) and D is the water diffusion coefficient (m^2/s). The pore tortuosity of the membrane is the deviation of the pore structure from the cylindrical shape, and can be calculated as follows, as suggested by Macki-Meares [3],

$$\tau = \frac{(2-\varepsilon)^2}{\varepsilon} \tag{4}$$

In addition, the value of PD ($Pa \cdot m^2/s$), which is the diffusivity of water vapor through the stagnant air inside the pores, can be given by [3,33,36].

$$PD = 1.895 \times 10^{-5} T_m^{2.072} \tag{5}$$

As the feed and permeate water vapor pressures within the membrane are not directly measurable, it is convenient to express Eq. (2) as [3,33,36,37]:

$$J_w = C_m\frac{dP}{dT}(T_{fm} - T_{pm}) \tag{6}$$

When the transmembrane bulk temperature difference is low $\left(T_{fm} - T_{pm} \le 10°C\right)$, the approximation $\frac{dP}{dT} = \frac{P_f - P_p}{\left(T_{fm} - T_{pm}\right)}$ can be made. As the membrane thickness is relatively small, the temperature difference across its surfaces can be assumed to be minimal. In Eq. (6), the term $\frac{dP}{dT}$ can be calculated by the Clausius-Clapeyron equation [3,36]:

$$\frac{dP}{dT} = \frac{\Delta H_v P_v}{RT_m^2} \tag{7}$$

where ΔH_v is the water latent heat of vaporization (J/mol), which can be estimated at the average membrane temperature, P_v (Pa) is the water vapor pressure of the feed solution. For low concentration solution, water vapor pressure can be calculated by using the Antoine equation [3,33,36].

$$P_0 = \exp\left(23.238 - \frac{3841}{T_m - 45}\right) \tag{8}$$

where P_0 (Pa) represents the vapor pressure of pure water at a given temperature. However, the vapor pressure also depends on the solution concentration (it increases with the increase of solution concentration). Therefore, Raoult's law can been utilized to determine the water vapor pressure of the feed solution, i.e. [38]:

$$P_v = (1 - x_i)P_0 \tag{9}$$

where x_i is the mole fraction of the solute in the feed solution.

The characteristics of electrospun nanofibrous membranes, such as the membrane thickness, mean pore size and porosity, for J_w and k_m calculation were shown in Table 1. The calculated J_w and C_m of electrospun PS-8–3 nanofibrous membranes were 40.36 kg/m^2h and 4.28×10^{-7} kg/$m^2 \cdot s \cdot Pa$ for using distilled water as the feed solution at 70 °C; 59.41 kg/m^2h and 4.22×10^{-7} kg/$m^2 \cdot s \cdot Pa$ for that at 80 °C. It was clear that the calculated J_w values of the electrospun PS-8–3 nanofibrous membrane were larger than the experimental values of the samples. This result may be explained by the fact that no effect of temperature polarization was assumed for calculation. In addition, these J_w values were calculated from the mean pore size of the electrospun membranes, where the maximum pore size and pore size distribution have not been considered properly. As a result, the experimentally measured J_w values for the electrospun PS-8–3 nanofibrous membranes are lowered than the theoretically calculated values. Comparisons on the mass transfer coefficient of the PS-8–3 membrane with some DCMD membranes in the literature were listed in Table 3 [3,36,37,39–42], which indicates that the electrospun PS nanofibrous membrane is a viable candidate for the MD operation.

3.4.2. Theoretical heat transfer analyses

It is well known that the heat transfer and mass transfer through the membrane occur simultaneously during the MD process. At the steady state, the overall heat transfer rate is equal

Table 3.
Comparison between the mass transfer coefficient of electrospun PS-8-3 nanofibrous membrane and those of other DCMD membranes from the literature.

DCMD Membranes	Pore size (μm)	Mass transfer coefficient (kg/m^2sPa)	Average temperature (T_m, °C)	Feed solution	Ref.
PTFE	0.2	14.5×10^{-7}	–	Distilled water	[3,39]
PTFE	0.45	21.5×10^{-7}	–	Distilled water	[3,39]
PVDF	0.22	3.8×10^{-7}	–	Distilled water	[3,40]
PVDF	0.45	4.8×10^{-7}	–	Distilled water	[37,41]
Enka PP	0.1	4.5×10^{-7}	–	Distilled water	[37,41]
Enka PP	0.2	4.3×10^{-7}	–	Distilled water	[37,41]
GVHP	0.22	5.4×10^{-7}	45	Distilled water	[42]
HVHP	0.45	7.5×10^{-7}	45	Distilled water	[42]
Immobilon	0.45	7.2×10^{-7}	45	Distilled water	[42]
TF200	0.23	10.2×10^{-7}	45	Distilled water	[36]
GVHP	0.27	3.8×10^{-7}	45	Distilled water	[36]
HVHP	0.45	4.7×10^{-7}	45	Distilled water	[36]
PS	0.19	4.3×10^{-7}	44	Distilled water	This study
PS	0.19	4.2×10^{-7}	49	Distilled water	This study

to the heat transfer rate in any of the three sections of the system: heat transfer in the feed solution (Q_f), heat transfer through the membrane (Q_m) and heat transfer on the permeate side (Q_p) [1,3,33,36,37].

The previous equations assume the knowledge of T_{fm} and T_{pm}, which actually differ from the measurable temperatures T_f and T_p because of the temperature polarization effect. Temperature polarization can be accounted for by calculating the heat transfer from each water channel to its respective membrane surface.

Heat transfer in the feed solution can be calculated according to the convection heat transfer equation [3,33,36,37],

$$Q_f = h_f(T_f - T_{fm}) \tag{10}$$

where $Q_f$is the total heat transfer in the feed layer, h_f is the heat transfer coefficient for the interface between the feed solution and the respective membrane wall, T_f is the temperature of the feed solution and $T_{fm}$is the temperature of the membrane at the interface between the membrane and the feed solution. The heat transfer through the membrane is divided into two parts, heat transfer by conduction across the membrane (i.e., polymer matrix and gas-filled pores), Q_c, and heat transferred by the latent heat of water vapor moving across the membrane, Q_v [3,33,36,37]. Conduction across the membrane serves no useful function and is considered heat loss, which should be minimized.

The latent heat transfer can be expressed as:

$$Q_v = J_w \Delta H_v = \Delta H_v C_m \frac{dP}{dT}(T_{fm} - T_{pm}) \tag{11}$$

while the conductive heat flux rate can be expressed as:

$$Q_c = \left(\frac{k_m}{\delta}\right)\left(T_{fm} - T_{pm}\right) \tag{12}$$

The thermal conductivity, k_m (W/mK) can be calculated from the conductivities of the membrane material and gas within its pores.

$$k_m = \varepsilon k_g + (1-\varepsilon)k_s \tag{13}$$

where k_g and k_s are thermal conductivities of the gas phase (i.e., water vapor) and the solid phase (i.e., membrane polymer materials). The total heat transfer across the membrane is the sum of the latent and conductive heat flux rate.

$$Q_m = Q_v + Q_c = \left(C_m \frac{dP}{dT}\Delta H_v + \left(\frac{k_m}{\delta}\right)\right)\left(T_{fm} - T_{pm}\right) = h_m\left(T_{fm} - T_{pm}\right) \tag{14}$$

where h_m represents the effective heat transfer coefficient of the membrane (W/m^{2}K).

The heat transfer by convection for the permeate side can be modeled similarly to the heat transfer on the feed side,

$$Q_p = h_p(T_{pm} - T_p) \tag{15}$$

where Q_p is the total heat transfer in the permeate solution, h_p is the heat transfer coefficient for the solution-membrane interface for the permeate side, T_p is the temperature of the permeate solution and T_{pm} is the temperature of the membrane at the respective interface between the membrane and the permeate stream. If the heat loss to the environment is negligible, the following relationships can be derived [33,36,37].

$$h_f\left(T_f - T_{f,m}\right) = \left(C_m \frac{dP}{dT}\Delta H_v + \left(\frac{k_m}{\delta}\right)\right)\left(T_{f,m} - T_{p,m}\right) = h_p\left(T_{p,m} - T_p\right) \tag{16}$$

Therefore, with some derivation, we can obtained

$$T_{fm} - T_{pm} = \frac{T_f - T_p}{1+\frac{h_m}{h_f}+\frac{h_m}{h_p}} = \psi(T_f - T_p) \tag{17}$$

where ψ is the temperature polarization coefficient which is $\frac{1}{1+\frac{h_m}{h_f}+\frac{h_m}{h_p}}$, representing how much of the thermal driving force $(T_f - T_p)$ contributes to the mass transfer force $(T_{fm} - T_{pm})$. The derived equations can be used to characterize membranes using experimental data.

$$h = \frac{1}{\frac{1}{h_f}+\frac{1}{h_p}} \tag{18}$$

$$J_w = C_m \frac{dP}{dT}(T_{fm} - T_{pm}) = C_m \frac{dP}{dT}\frac{(T_f - T_p)}{1+\frac{h_m}{h}} \tag{19}$$

Substituting with the relationships $h_m = C_m \frac{dP}{dT}\Delta H_v + \left(\frac{k_m}{\delta}\right)$ and $\Delta T = (T_f - T_p)$, we get

$$\frac{\Delta T}{J_w \Delta H_v} = \frac{1}{dP/dT}\frac{1}{C_m \Delta H_v}\left(1+\frac{k_m}{\delta h}\right) + \frac{1}{h} \tag{20}$$

Plotting $\frac{\Delta T}{J_w \Delta H_v}$ vs. $\frac{1}{\frac{dP}{dT}}$ should yield a slope of $\left(\frac{1}{C_m \Delta H_v}\right)\left(1+\frac{k_m}{\delta}h\right)$ and an intercept at $\frac{1}{h}$, from which h can be obtained [36].

$U$is the overall heat transfer coefficient [33], having the following expression:

$$U = \frac{1}{\frac{1}{h_f}+\frac{1}{h_m}+\frac{1}{h_p}} = \frac{1}{\frac{1}{h_m}+\frac{1}{h}} \tag{21}$$

The experimental J_w values of electrospun PS-8-3 nanofibrous membranes obtained from trials using the distilled water as feed solution at 70 °C and 80 °C were 26.9 ± 0.5 kg/m$^2 \cdot$h and 33.7 ± 0.6 kg/m$^2 \cdot$h, respectively. Based on the experimental J_w values, the membranes heat transfer coefficient (h_m) of the PS-8-3

Table 4.
Comparison between the heat transfer coefficient of electrospun PS-8-3 nanofibrous membrane and those of other DCMD membranes from the literature.

DCMD Membranes	Pore size (μm)	Heat transfer coefficient (W/m^{2}K)	Average temperature (T_m, °C)	Feed solution	Ref.
TF200	0.23	3100	55	Distilled water	[36]
GVHP	0.27	3500	55	Distilled water	[36]
HVHP	0.45	4600	55	Distilled water	[36]
PVDF	0.45	2490	60	Distilled water	[37]
Enka PP	0.1	2440	60	Distilled water	[37]
Enka PP	0.2	2380	60	Distilled water	[37]
PS	0.19	2693	44	Distilled water	This study
PS	0.19	3330	49	Distilled water	This study

membrane and overall heat transfer coefficient (U) of the system could be calculated: 2693.1 W/m$^2\cdot$K and 394.69 W/m$^2\cdot$K for 70 °C feed solution; 3329.7 W/m$^2\cdot$K and 406.07 W/m$^2\cdot$K for 80 °C feed solution, respectively. Table 4 were summarized the heat transfer coefficient of the PS-8–3 nanofibrous membrane and its comparison with some DCMD membranes reported in the literature under the similar experimental conditions [36,37].

4. Conclusions

A series of hydrophobic electrospun PS nanofibrous membranes with average fiber diameter ranging from about 240 ± 11 nm to 150 ± 8 nm were successfully prepared by electrospinning from solutions with the concentration range between 8 wt% and 12 wt%. SEM images illustrated that the morphological structure of electrospun PS nanofibers changed from beaded nanofibers to bead-free nanofibers after the addition of 0.5 wt% SDS. The results from SEM and porometer suggested that the average fiber diameter and membranes thickness can dramatically affect the mean pore size, pore size distribution of PS nanofibrous membranes. The optimized PS-8–3 nanofibrous membrane had reasonably high porosity (84%), narrow pore size distribution and suitable average pore size (about 0.19 μm), good water contact angle (about 114°) for the DCMD operation, where its filtration performance was comparable or better than commercially available PTFE membranes tested with four different kinds of feed solution. The permeate flux rate of the PS nanofibrous membranes was found to increase with the increase of feed temperature and flow rate, as well as the decrease of saline concentration in the feed solution. The average permeate flux rate of the optimized PS-8–3 nanofibrous membrane was about 31.05 ± 0.60 kg/m$^2\cdot$h over a 10 h of DCMD operation (using feed solution: 35 g/L NaCl; feed and cold solutions temperatures: 80 °C and 17 °C; flow rate: 0.2 GPM), while maintaining the stable permeate water conductivity (lower 5 us/cm). The calculated mass and heat transfer coefficients of the optimized PS-8-3 nanofibrous membrane were 4.28×10^{-7} kg/m$^2\cdot$s$\cdot$Pa and 2693.1 W/m$^2\cdot$K using distilled water as the feed solution at 70 °C; and 4.22×10^{-7} kg/m$^2\cdot$s$\cdot$Pa and 3329.7 W/m$^2\cdot$K at 80 °C. These results are comparable to those of typical membranes for the MD operation. This study confirmed that electrospun PS nanofibrous membranes with the mean pore size less than 0.19 μm can be used as effectively in DCMD to purify brackish and seawater.

Acknowledgements

This research was financially supported by a grant from the King AbdulAziz City for Science and Technology, and a SusChEM award from the National Science Foundation in the U. S. (DMR-1409507).

Nomenclature

C_m	mass transfer coefficient of the membrane (kg/m$^2\cdot$s$\cdot$Pa).
D	water diffusion coefficient (m^2/s).
d_e	collision diameter of water vapor molecule (m).
ΔH_v	water latent heat of vaporization (J/mol).
h_m	effective heat transfer coefficient of the membrane (W/m$^2\cdot$K).
h_f	heat transfer coefficient for the interface between the feed solution and the membrane wall (W/m$^2\cdot$K).
h_p	heat transfer coefficient for the interface between the permeate solution and membrane wall (W/m$^2\cdot$K).
J_w	mass flux rate (kg/m$^2\cdot$h).
k_n	Knudsen number (-).
k_B	Boltzmann constant (J/K).
k_g	thermal conductivities of the water vapor within membrane pores (W/m$\cdot$K).
k_s	thermal conductivities of the membrane material (W/m$\cdot$K).
M_w	molecular weight of water (kg/mol).
PD	diffusivity of water vapor through the stagnant air inside the pores (Pa$\cdot$m^2/s).
P	total pressure inside the membrane pores (Pa).
P_a	air pressure inside the membrane pores (Pa).
P_v	water vapor pressure inside the membrane pores (Pa).
P_{ave}	average pressure within the membrane pores (Pa).
P_f	water vapor pressure on feed solution side of the membrane (Pa).
P_p	water vapor pressure on permeate solution side of the membrane (Pa).
P_0	water vapor pressure of pure water at a given temperature (Pa).
Q_f	heat transfer by convection in the feed boundary layer (W/m^2).
Q_m	heat transfer through the membrane (W/m^2).
Q_p	heat transfer by convection in the permeate boundary layer (W/m^2).
Q_c	heat transfer by conduction across the membrane (W/m^2).
Q_v	heat transfer by latent heat of vaporization across the membrane (W/m^2).
R	gas constant (J/K$\cdot$mol).
T_m	average temperature of the membrane (K).
T_f	feed solution temperature (K).
T_p	permeate solution temperature (K).
T_{fm}	surface temperature on feed solution side of the membrane (K).
T_{pm}	surface temperature on permeate solution side of the membrane (K).
U	overall heat transfer coefficient (W/m$^2\cdot$K).
x_i	mole fraction of the solute in the feed solution (-).

Greek symbol

λ	mean free path of water vapor (m).
δ	membrane thickness (m).
τ	pore tortuosity (%).
ε	porosity (%).
r	pore radius (m).
ψ	temperature polarization coefficient (-).

References

[1] K.W. Lawson, D.R. Lloyd, Membrane distillation, J. Membr. Sci. 124 (1997) 1–25.
[2] M. Khayet, Membranes and theoretical modeling of membrane distillation: A review, Adv. Colloid Interfac. 164 (2011) 56–88.
[3] A. Alkhudhiri, N. Darwish, N. Hilal, Membrane distillation: A comprehensive review, Desalination 287 (2012) 2–18.
[4] S.T. Hsu, K.T. Cheng, J.S. Chiou, Seawater desalination by direct contact

membrane distillation, Desalination 143 (2002) 279–287.
[5] A. Kullab, A. Martin, Membrane distillation and applications for water purification in thermal cogeneration plants, Sep. Purif. Technol. 76 (2011) 231–237.
[6] M. Tomaszewska, M. Gryta, A.W. Morawski, Study on the concentration of acid by membrane distillation, J. Membr. Sci. 102 (1995) 113–122.
[7] S. Gunko, S. Verbych, M. Bryk, N. Hilal, Concentration of apple juice using direct contact membrane distillation, Desalination 190 (2006) 117–124.
[8] M. Gryta, M. Tomaszewska, K. Karakulski, Wastewater treatment by membrane distillation, Desalination 198 (2006) 67–73.
[9] A.O. Imdakm, T. Matsuura, Simulation of heat and mass transfer in direct contact membrane distillation (MD): The effect of membrane physical properties, J. Membr. Sci. 262 (2005) 117–128.
[10] A. Greiner, J.H. Wendorff, Electrospinning: A fascinating method for the preparation of ultrathin fibers, Angew. Chem. Int. Ed. 46 (2007) 5670–5703.
[11] V. Beachley, X.J. Wen, Effect of electrospinning parameters on the nanofiber diameter and length, Mater. Sci. Eng. C 29 (2009) 663–668.
[12] I.S. Chronakis, Novel nanocomposites and nanoceramics based on polymer nanofibers using electrospinning process-A review, J. Mater. Process Tech 167 (2005) 283–293.
[13] H.T. Zhu, S.S. Qiu, W. Jiang, D.X. Wu, C.Y. Zhang, Evaluation of electrospun polyvinyl chloride/polystyrene fibers as sorbent materials for oil spill cleanup, Env. Sci. Technol. 45 (2011) 4527–4531.
[14] X. Li, C. Wang, Y. Yang, X.F. Wang, M.F. Zhu, B.S. Hsiao, Dual-biomimetic superhydrophobic electrospun polystyrene nanofibrous membranes for membrane distillation, ACS Appl. Mater. Inter 6 (2014) 2423–2430.
[15] H.Y. Ma, C. Burger, B.S. Hsiao, B. Chu, Ultra-fine cellulose nanofibers: new nano-scale materials for water purification, J. Mater. Chem. 21 (2011) 7507–7510.
[16] C.M. Hsu, S. Shivkumar, Nano-sized beads and porous fiber constructs of poly (ε-caprolactone) produced by electrospinning, J. Mater. Sci. 39 (2004) 3003–3013.
[17] Z.M. Huang, Y.Z. Zhang, M. Kotaki, S. Ramakrishna, A review on polymer nanofibers by electrospinning and their applications in nanocomposites, Compos Sci. Technol. 63 (2003) 2223–2253.
[18] C. Mituppatham, M. Nithitanakul, P. Supaphol, Ultrafine electrospun polyamide-6 fibers: effect of solution conditions on morphology and average fiber diameter, Macromol. Chem. Phys. 205 (2004) 2327–2338.
[19] P. Heikkila, A. Harlin, Parameter study of electrospinning of polyamide-6, Eur. Polym. J. 44 (2008) 3067–3079.
[20] L.D. Tijing, Y.C. Woo, M.A.H. Johir, J.S. Choi, H.K. Shon, A novel dual-layer bicomponent electrospun nanofibrous membrane for desalination by direct contact membrane distillation, Chem. Eng. J. 256 (2014) 155–159.
[21] L.D. Tijing, Y.C. Woo, W.G. Shim, T. He, J.S. Choi, S.H. Kim, H.K. Shon, Superhydrophobic nanofiber membrane containing carbon nanotubes for high-performance direct contact membrane distillation, J. Membr. Sci. 502 (2016) 158–170.
[22] J.A. Prince, G. Singh, D. Rana, T. Matsuura, V. Anbharasi, T. S. Shanmugasundaram, Preparation and characterization of highly hydrophobic poly(vinylidene fluoride)-Clay nanocomposite nanofiber membranes (PVDF-clay NNMs) for desalination using direct contact membrane distillation, J. Membr. Sci. 397–398 (2012) 80–86.
[23] C.L. Su, J.H. Shih, M.S. Huang, C.M. Wang, W.C. Shih, Y.S. Liu, A study of hydrophobic electrospun membrane applied in seawater desalination by membrane distillation, Fiber Polym. 13 (2012) 698–702.
[24] M.W. Yao, Y.C. Woo, L.D. Tijing, W.G. Shim, J.S. Choi, S.H. Kim, H.K. Shon, Effect of heat-press conditions on electrospun membranes for desalination by direct contact membrane distillation, Desalination 378 (2016) 80–91.
[25] B.S. Lalia, E.G. Burrieza, H.A. Arafat, R. Hashaikeh, Fabrication and characterization of polyvinylidenefluoride-co-hexafluoropropylene (PVDF-HFP) electrospun membranes for direct contact membrane distillation, J. Membr. Sci. 428 (2013) 104–115.
[26] Y. Liao, C.H. Loh, R. Wang, A.G. Fane, Electrospun superhydrophobic membranes with unique structures for membrane distillation, ACS Appl. Mater. Inter 6 (2014) 16035–16048.
[27] X. Li, X.F. Yu, C. Cheng, L. Deng, M. Wang, X.F. Wang, Electrospun superhydrophobic organic/inorganic composite nanofibrous membranes for membrane distillation, ACS Appl. Mater. Inter 7 (2015) 21919–21930.
[28] Y. Liao, R. Wang, A.G. Fane, Fabrication of bioinspired composite nanofiber membranes with robust superhydrophobicity for direct contact membrane distillation, Env. Sci. Technol. 48 (2014) 6335–6341.
[29] Y. Liao, R. Wang, A.G. Fane, Engineering superhydrophobic surface on poly (vinylidene fluoride) nanofiber membranes for direct contact membrane distillation, J. Membr. Sci. 440 (2013) 77–87.
[30] Y. Liao, R. Wang, M. Tian, C.Q. Qiu, A.G. Fane, Fabrication of polyvinylidene fluoride (PVDF) nanofiber membranes by electro-spinning for direct contact membrane distillation, J. Membr. Sci. 425–426 (2013) 30–39.
[31] M. Essalhi, M. Khayet, Self-sustained webs of polyvinylidene fluoride electrospun nanofibers at different electrospinning times: 1. Desalination by direct contact membrane distillation, J. Membr. Sci. 433 (2013) 167–179.
[32] M. Essalhi, M. Khayet, Self-sustained webs of polyvinylidene fluoride electrospun nano-fibers: effects of polymer concentration and desalination by direct contact membrane distillation, J. Membr. Sci. 454 (2014) 133–143.
[33] M. Qtaishat, T. Matsuura, B. Kruczek, M. Khayet, Heat and mass transfer analysis in direct contactmembrane distillation, Desalination 219 (2008) 272–292.
[34] S. Srisurichan, R. Jiraratananon, A.G. Fane, Mass transfer mechanisms and transport resistances in direct contact membrane distillation process, J. Membr. Sci. 277 (2006) 186–194.
[35] Z. Dong, R. Ma, A.G. Fane, A new model for mass transfer in direct contact membrane distillation, Desalination 151 (2002) 217–227.
[36] M. Khayet, A. Velazquez, J.I. Mengual, Modelling mass transport through a porous partition: effect of pore size distribution, J. Non-Equil Thermody. 29 (2004) 279–299.
[37] R.W. Schofield, A.G. Fane, C.J.D. Fell, Heat and mass transfer in membrane distillation, J. Membr. Sci. 33 (1987) 299–313.
[38] A. Boubakri, A. Hafiane, S.A.T. Bouguecha, Direct contact membrane distillation: Capability to desalt raw water, Arab. J. Chem. 4 (2014) 557–563.
[39] M.C. Garcia-Payo, M.A. Izquierdo-Gil, F. Pineda, Wetting study of hydrophobic membranes via liquid entry pressure measurements with aqueous alcohol solutions, J. Colloid Interf. Sci. 230 (2000) 420–431.
[40] A.O. Imdakm, A.O. Imdakm, T. Matsuura, A monte carlo simulation model for membrane distillation processes: direct contact (MD), J. Membr. Sci. 237 (2004) 51–59.
[41] P.P. Zolotarev, V.V. Ugrozov, I.B. Volkina, V.M. Nikulin, Treatment of waste water for removing heavy metals by membrane distillation, J. Hazard Mater. 37 (1994) 77–82.
[42] L. Martinez, F.J. Florido-Diaz, A. Hernandez, P. Pradanos, Estimation of vapor transfer coefficient of hydrophobic porous membranes for applications in membrane distillation, Sep. Purif. Technol. 33 (2003) 45–55.